**Author's post print version**

*Mauro Torquati, Andrea Belleri & Paolo Riva (2018) Displacement-Based Seismic Assessment for Precast Concrete Frames with Non-Emulative Connections, Journal of Earthquake Engineering, DOI: 10.1080/13632469.2018.1475311*

*Publisher's version: http://dx.doi.org/10.1080/13632469.2018.1475311*

# Displacement based seismic assessment for precast concrete frames with non-emulative connections

Mauro Torquati, Andrea Belleri[1], Paolo Riva

**Abstract**

The paper develops a methodology for the seismic vulnerability assessment, Displacement Based Assessment (DBA), of one-storey and multi-storey precast concrete frames with non-emulative connections. The method is based on the Direct Displacement Based Design procedure initially developed by Priestley. The DBA is particularly suitable for the evaluation of the seismic response of flexible structures, as it considers displacements as the leading parameters to estimate the seismic vulnerability. The proposed procedure specifically accounts for the influence of beam-column connections, P-Δ effects and second mode of vibration. The validation has been performed by means of nonlinear time history analyses.

**Keywords**:

Displacement Based Assessment; Precast Structure; Non-emulative connections; Inelastic Deflected Shape; P-Δ effects.

[1] Assistant Professor, Dept. of Engineering and Applied Sciences, University of Bergamo, Italy; corresponding author - andrea.belleri@unibg.it

## 1. Introduction

Precast construction technology is widely adopted thanks to the many advantages deriving from its simplicity and versatility. In Italy, reinforced concrete (RC) precast buildings are commonly used for industrial and commercial facilities, usually adopting non-emulative dry connections to assemble the different elements. In areas not originally classified as seismic zones prior to 2004, structures were not designed for seismic loads. For these types of buildings, the achievement of a structural behaviour like cast in place RC buildings is difficult, unless the so called "emulative" connections were used.

In the seismic assessment of existing buildings, the considered structures are generally treated as hinged frames with cantilever columns fix-connected at the base, although the performance of beam-column connections (Brunesi et al. 2015, Magliulo et al. 2015, Zoubek et al. 2013, Palanci et al. 2017, Kremmyda et al. 2017) should be included in the assessment for a better estimation of the structural vulnerability. The considered structures are very flexible and characterized by a high seismic displacement demand because of large inter-storey heights and slenderness of the columns. This leads to a seismic performance typically governed by the inter-storey displacement control rather than by the limitation of material strains.

In the case of properly detailed connections and considering the high quality deriving from the excellent standard achieved in the production process, precast structures could achieve high performances in the case of earthquakes. However, due to a design carried out before the enforcement of modern building code regulations and before an updated seismic zonation of the Italian territory, many existing buildings are characterized by inadequate construction details and poor seismic performance.

The high seismic vulnerability of existing precast buildings has been clearly highlighted by past seismic events on the Italian territory (Toniolo and Colombo 2012, Magliulo et al. 2013, Belleri et al. 2015a, Belleri et al. 2015b, Minghini et al. 2016, Clementi et al. 2016, among others). The main damage patters observed are associated with failure of structural and non-structural connections, such as cladding panels (Scotta et al. 2015, Belleri et al. 2016), loss of beam supports (Casotto et al. 2015, Ercolino et al. 2016), poor detailing in the columns and absence of floor/roof diaphragm action. It is worth noting that failure of the connections was the factor leading to most of the recorded collapses. Therefore, an accurate evaluation of the seismic vulnerability of precast structures should account for precast connections.

In this paper, a seismic vulnerability assessment procedure is investigated. Such procedure, namely Displacement Based Assessment (DBA), has been derived following the Direct Displacement Based Design (DDBD) methodology initially developed by Priestley (Priestley 1997, Priestley et al. 2007) and extended to precast frame structures by Belleri (2017b). The procedure considers building lateral displacements as the main parameters for the seismic assessment of the structure (Sullivan and Calvi 2013, Welch et al. 2014, Landi et al. 2016, Cardone 2016). The lateral displacement is a suitable seismic vulnerability indicator for the considered buildings, due to the high deformability of the structural system combined with the high deformation demand in the connection region.

The procedure is developed for one-storey and multi-storey precast RC frames and accounts for the main aspects influencing the seismic behaviour of the structure.,

The influence of non-emulative connections is specifically included in the definition of the distribution of seismic forces and deformations, being the connections one of the most vulnerable

elements and the major cause of collapse of existing precast buildings. In addition, the influence of second order (P-Δ) effects and the second mode of vibration are directly considered.
The proposed DBA procedure is applied to selected case studies representing a 3-storey frame of a multi-storey RC precast building. The results are validated by means of nonlinear time history analyses.

## 2. Displacement Based Assessment procedure

A vulnerability assessment procedure in accordance with the Direct Displacement Based Design approach (Priestley 1997, Priestley et al. 2007) is presented herein. Such an approach represents a more rational choice compared to typical force based design approaches, being structural damage strain related, and strains associated with displacements. A scheme of the DDBD approach is represented in **Figure 1**, the reader is referred to Priestley et al. 2007 and to Belleri (2017b) for the application to precast concrete structures. The DDBD considers a deflected shape representing the first inelastic mode of vibration; then an elastic equivalent single-degree-of-freedom (SDOF) structure is defined, with stiffness equal to the secant stiffness at maximum displacement. Based on the displacement ductility, the equivalent viscous damping (EVD) of the substitute system is defined and the elastic displacement spectrum at 5% damping is reduced accordingly; this allows obtaining the effective period of the equivalent SDOF system, the related stiffness and the base shear. The base shear is finally distributed along the building height and the load demand in the structural elements evaluated accordingly.

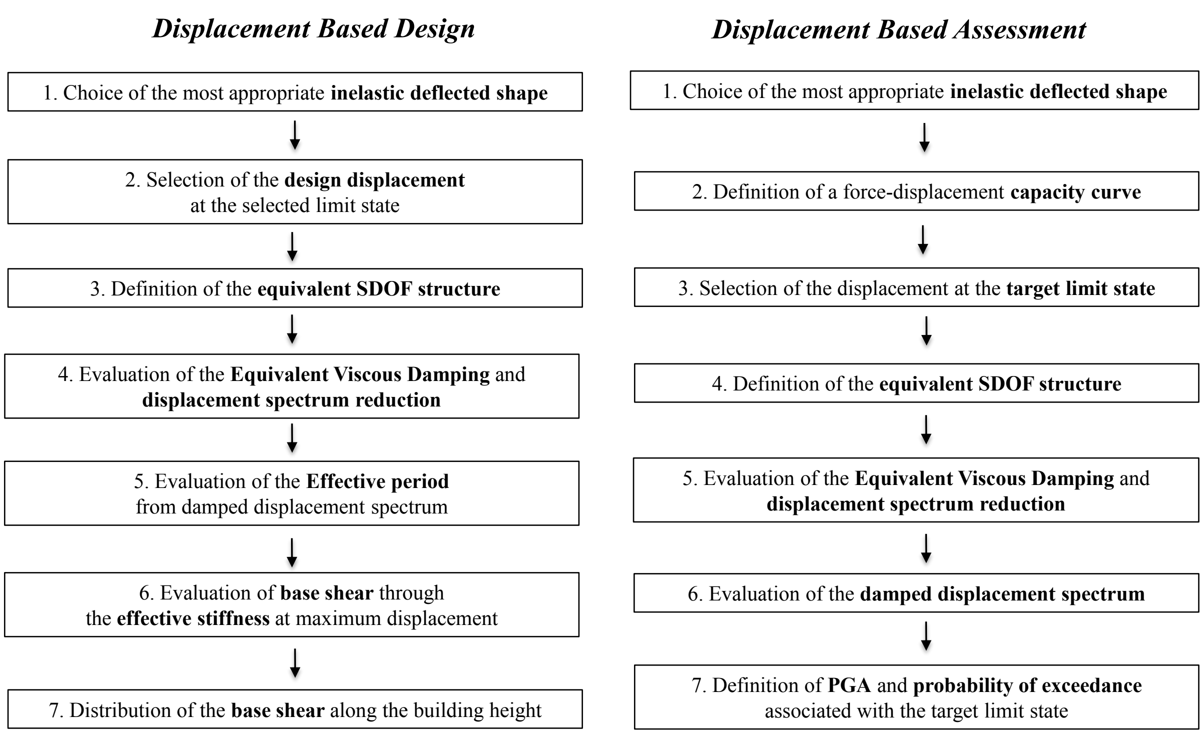


***Figure 1*** *– Schematic representation of DBD and DBA procedures*

The DBA procedure is developed in accordance with the aforementioned principles (Figure 1). An in-depth explanation of the main steps is presented in the following. In addition, it is worth noting that the DBA procedure could be applied in a different sequence of steps, to suit the engineer or structure in question, without affecting the core principles of the approach.

*Steps 1 to 3: from the inelastic deflected shape to the limit state selection*

In Step 1, an appropriate inelastic deflected shape is defined. The system non-linearity is examined to understand the most probable inelastic mechanisms. This step is particularly critical as it influences the entire procedure and its reliability, since it drives the definition of the parameters of the equivalent SDOF structure. Herein, two different methods are proposed for the definition of the inelastic deflected shape: the Pushover Method (PM) and the Equivalent Column Simplified Method (ECSM). In Step 2, a force-displacement capacity curve is derived from the obtained inelastic deflected shapes. In Step 3, a limit state corresponding to a point in the capacity curve is selected. Such limit state will be considered to estimate the probability of exceedance.
The base shear and the lateral displacement at each floor are evaluated at yielding of the system ($V_y$ , $\Delta_{y,i}$) and at the selected limit state ($V_u$ , $\Delta_{u,i}$). The PM and ECSM procedures are described in the next section.

*Step 4: Substitute structure parameters*

The parameters of the equivalent SDOF structure are defined in **Table 1**.

***Table1*** *- Definition of the parameters of the equivalent SDOF structure*
*Note: $m_i$ is the mass of the $i^{th}$ floor;*
*$\Delta_{y,i}$ , $\Delta_{u,i}$ are the displacements at yield and at the selected limit state for the $i^{th}$ floor, respectively.*

| | | | |
|---|---|---|---|
| Yield displacement | $\Delta_{y,SDOF} = \dfrac{\sum m_i \cdot \Delta_{y,i}^2}{\sum m_i \cdot \Delta_{y,i}}$ | | (1) |
| Target displacement | $\Delta_{u,SDOF} = \dfrac{\sum m_i \cdot \Delta_{u,i}^2}{\sum m_i \cdot \Delta_{u,i}}$ | | (2) |
| Effective mass | $m_{eff} = \dfrac{\sum m_i \cdot \Delta_{u,i}}{\Delta_{u,SDOF}}$ | | (3) |
| Secant stiffness at target displacement | $k_{eff} = \dfrac{V_u}{\Delta_{u,SDOF}}$ | 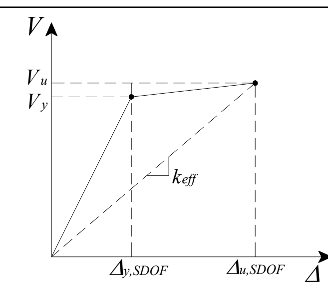 | (4) |
| Effective period | $T_{eff} = 2\pi\sqrt{\dfrac{m_{eff}}{k_{eff}}}$ | | (5) |

*Step 5: Equivalent viscous damping (EVD) and Displacement Spectrum reduction*

The equivalent structure corresponds to an elastic SDOF system with a fundamental period of vibration ($T_{eff}$) obtained from considering the secant stiffness of the inelastic structure at maximum displacement ($\Delta_{u,SDOF}$). The EVD of the equivalent structure is associated with the hysteretic energy dissipation of the structural system (Priestley et al. 2007, Dwairi et al. 2007, Grant et al. 2004, Belleri 2017b). In the case of RC structures, the material nonlinearity is well captured by the Takeda (Otani 1974) model, whose corresponding EVD ($\xi_{eq}$) is a function of the displacement ductility $\mu_\Delta$, defined as $\Delta_{u,SDOF}/ \Delta_{y,SDOF}$:

$$\xi_{eq} = 0.05 + \alpha\left(\frac{\mu_\Delta - 1}{\mu_\Delta \pi}\right) \tag{6}$$

where $\alpha$ depends on the structural system (e.g. frame buildings or wall buildings). **Eq.6** allows obtaining a damped displacement spectrum ($S_{D,in}$) accounting for viscous damping values different from 5%:

$$\eta = \frac{S_{D,in}\left(T, \xi_{eq}\right)}{S_{D,el}\left(T, \xi = 0.05\right)} = \sqrt{\frac{0.05 + z}{z + \xi_{eq}}} \tag{7}$$

It is important to highlight that the coefficients $\alpha$ and $z$ in **Eq.6** and **Eq.7** depend on the ground motion set used in the calibration of each equation; nonetheless, when the equations are combined, independent results are obtained if the same ground motion set is used in the calibration of each equation (Pennucci et al. 2011). Therefore, considering the formula for the damped displacement spectrum contained in EN 1998-1 (i.e. **Eq.7** with $z$=0.05), the corresponding values of $\alpha$ are 0.635 and 0.808 for wall and frame buildings, respectively. Such values have been obtained from Priestley et al. (2007) by means of a least square regression analysis; indeed, the values of $\alpha$ (0.444 and 0.565 for the wall and frame buildings, respectively) contained in Priestley et al. (2007) are associated with $z$=0.02 in **Eq.7**.

The present paper considers **Eq.7** with $z$=0.05 and **Eq.6** with $\alpha$=0.635. The deflected shape and energy dissipation capacity of the structural typology under investigation (i.e. non-emulative beam-column connections) are closer to wall buildings rather than frame buildings. **Eq.6** is considered appropriate for a first estimate of EVD. For a refined EVD estimate, including the peculiar hysteretic shape of beam-column connections, a detailed evaluation should be carried out, following for instance what reported in Belleri (2017b) or other algorithms.

*Step 6 and 7: Damped displacement spectrum and probability of exceedance*

$\Delta_{u,SDOF}$ and $T_{eff}$ identify a point in the damped displacement spectrum (**Figure 2**). The related elastic displacement spectrum is obtained from **Eq.6** and **Eq.7** (Step 6). Once the elastic displacement spectrum has been defined, the probability of exceedance associated with the selected limit state is obtained from building code formulations, as in EN 1998-1 (Step 7).

To account for uncertainty in the DBA procedure (Sullivan and Calvi, 2013), the simplified procedure proposed by Fajfar and Dolsek (2012) could be adopted. Finally, P-Δ effects and the second mode of vibration influence the response of the equivalent SDOF system; to account for such effects in the DBA approach, specific procedures have been developed and addressed in the following.

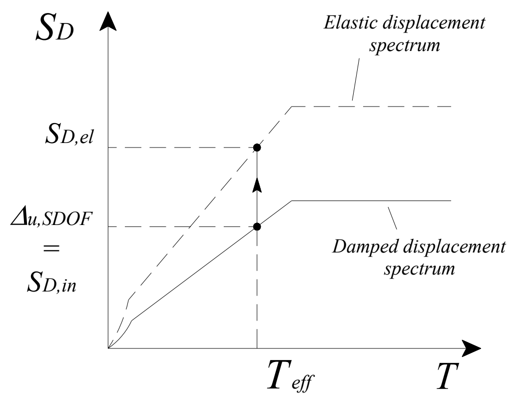


***Figure2*** *– Relationship between elastic and damped displacement spectrum*

## 3. Displacement profile and capacity curve definition

The definition of the probable displacement profile of the structure in the non-linear range represents one of the key steps in the DBA procedure. Priestley et al. (2007) provided formulations for the definition of the inelastic deformed shape for the most common structural systems. Such formulations are suitable for the design of new structures, where capacity design enforces the structure to behave in a controlled ductile manner. In the case of existing structures not designed following modern anti-seismic approaches, as the construction typology analysed herein, a simplified estimation of the displacement profile represents a critical task. In addition, it is worth noting that the connections between the elements may influence the nonlinear behaviour of the whole system: indeed, beam-column connections could significantly affect the inelastic displacement distribution, with possible displacement compatibility issues between the connected elements (Belleri et al. 2014, Belleri et al. 2015b, Belleri et al. 2016).
This paper proposes two methods to obtain the displacement profile of existing precast structures with non-emulative connections: an accurate approach (Pushover Method - PM), requiring non-linear finite element analyses, and a simpler approach (Equivalent Column Simplified Method - ECSM), based on simplified assumptions and formulations. It is worth noting that in the absence of mechanical connections between beams and columns or between floor elements and supporting beams, i.e. connections relying on friction, specific time history analyses should be carried out including the vertical component of the ground motion to evaluate the possibility of loss of support.

### *3.1 Pushover Method (PM)*

In the first method, the definition of the inelastic deflected shape is performed by means of classical or adaptive pushover analyses. The non-linear behaviour of both RC structural elements and connections is directly accounted for, being the latter specifically addressed in the next section. The resulting capacity curve, in terms of base shear versus roof displacement, is bilinearized according to current standards (herein EN 1998-1). This allows defining the displacement and base shear at yield ($\Delta_y$, $V_y$) and at the target limit state ($\Delta_u$, $V_u$). The associated floor displacements ($\Delta_{y,i}$ and $\Delta_{u,i}$) are recorded and the equivalent SDOF structure is defined as described in the previous section.

A nonlinear finite element model allows accounting for specific aspects not considered in the following simplified approach (ECSM), as for instance the diaphragm flexibility and the presence of infills (masonry infills and cladding panels interacting with the structure). The diaphragm flexibility is directly evaluated in the pushover analysis by a three-dimensional finite element model including the connections between floor elements and the possible RC cast-in-place topping. Regarding masonry infills, they can be considered by means of simplified struts as in El-Dakhakhni et al. 2003, Crisafully and Carr 2007, and Rodrigues et al. 2010 among others. In the case of external precast cladding panels, the panel-structure connections are typically characterized by high vulnerability due to lack of in-plane displacement compatibility of the connecting system (Brunesi et al. 2015, Belleri et al. 2016, Zoubek et al. 2016, Toniolo and Dal Lago 2017), which leads to a generally low bracing contribution. Therefore, in such conditions, a prediction of the performance of the cladding panel connections could be carried out without modelling the connecting system but just considering the relative displacements between the connecting points.

*3.2 Equivalent column simplified method (ECSM)*

ECSM has been developed to provide a faster and simplified evaluation of the displacement profile of one-storey, two-storey and three-storey precast frames under seismic loading without requiring finite element modelling. The following assumptions apply:

i. the columns are continuous up to the roof;
ii. the beams flexure stiffness is much higher than the joint rotational stiffness (i.e. the flexural deformations are lumped at the beam-column non-emulative connection);
iii. the post-yield stiffness of columns and connections is zero;
iv. all the connections are considered yielded after first yielding of any connection.

The simplified procedure leads to the definition of an approximate capacity curve for planar frames, therefore it is not intended to capture three-dimensional effects such as those related to diaphragm flexibility or the influence of rigid infills, which require more refined analyses. However, this procedure has the advantage of not requiring finite element analyses, because it is based on the step by step application of analytical formulations. The procedure can be implemented in spreadsheets and can be seen as a seismic screening tool for a rapid assessment of the structural vulnerability. In general, seismic screening has the advantage of highlighting potential seismic deficiencies and it is adopted both to rank the seismic vulnerability of buildings among a portfolio and to get a preliminary estimate of the seismic risk of a given building. FEMA 154 and ASCE/SEI 41 are examples of seismic screening procedures. ECSM considers an equivalent column system. **Figure 3** shows the schemes used to represent one-storey, two-storey and three-storey precast frames. ECSM assumes that the behaviour of the building can be represented by a planar model. Displacement amplifications due to accidental eccentricity could be added in the same way of building code formulations.

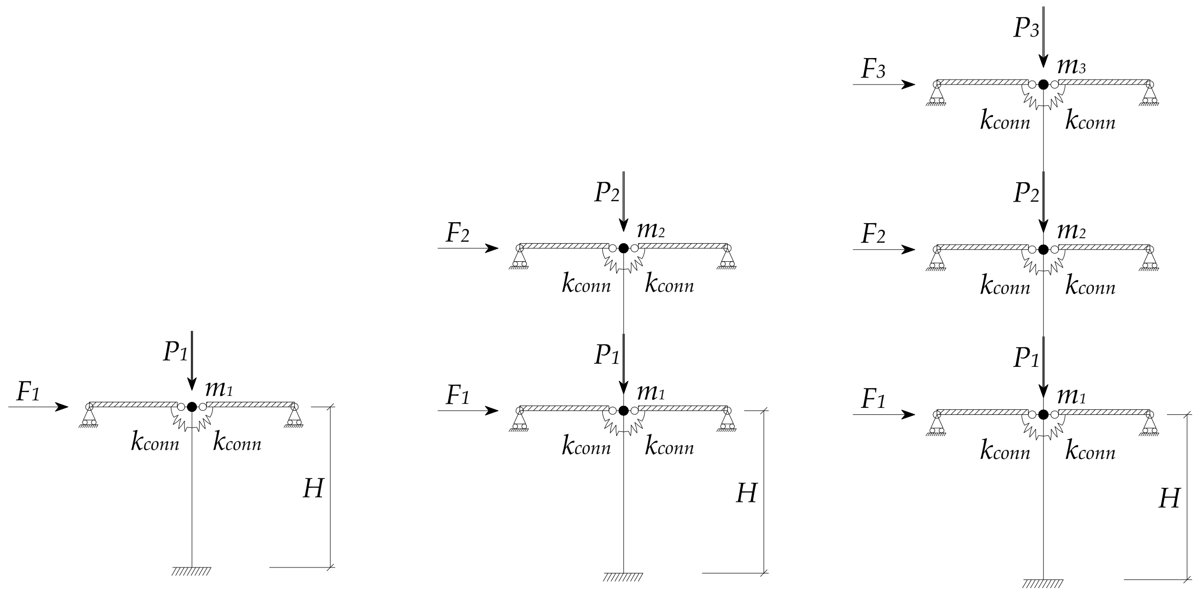


***1-Storey*** ***2-Storey*** ***3-Storey***

***Figure 3*** *–Simplified schemes considered for the application of the procedure*
*Note: $F_i$ is the storey load proportional to the first mode eigenvector;*
*$P_i$ and $m_i$ are the floor vertical load and the seismic mass, respectively;*
*$k_{conn}$ is the stiffness of beam-column connections*

*Step 1: Lateral load distribution*

The lateral load distribution is related to the fundamental vibration mode of the building. The rotational stiffness of the beam-column joints is initially neglected, as in an ideal hinged-frame structure; in this configuration the lateral load resisting systems is made of cantilever columns. The horizontal forces $F_i$ on the system are proportional to $\phi_i\ m_i$, where $m_i$ is the floor mass and $\phi_i$ corresponds to the i[th] eigenvector component of the first mode of vibration of the considered equivalent column. In the case of a continuous column with constant cross-section, constant inter-storey height and constant floor-mass, the eigenvector of the fundamental mode is independent from the column height and column cross-section. In such case, the eigenvector components are reported in **Figure 4**.

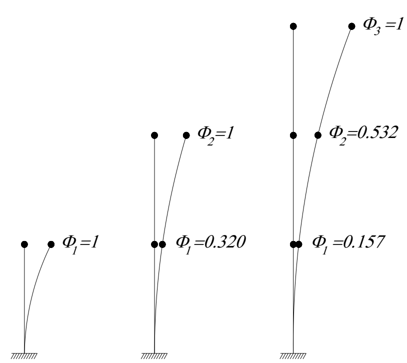


***Figure 4*** *– Eigenvectors of cantilever column for one-storey, two-storey, and three-storey*

*Step 2: Influence of beam-column connections*

The influence of beam-column connections on displacements and rotations is considered herein. Reference is made to the values obtained from the hinged-frame column mentioned in the previous step. A parametric analysis has been performed to define displacements and rotations as a function of the connection stiffness, considering the lateral load distribution proportional to the eigenvector accounting for the connection stiffness. **Figure 5** shows the results of the analyses in terms of displacements and rotations at each floor ($\Delta_i$, $\varphi_i$, respectively) in dimensionless form. In the figure, displacements and rotations obtained from a load distribution according to the first mode of vibration including connection stiffness are normalized to those corresponding to the cantilever column case ($\Delta_{i,0}$, $\varphi_{i,0}$) obtained from a load distribution according to the first mode of vibration depicted in **Figure 4;** it is worth noting that the former load distribution has been previously scaled in order to have the same base shear of the latter. The connection stiffness ($k_{conn}$) is normalized by *(EI)/H*, where *H, E* and *I* are the inter-storey height, the modulus of elasticity and the second moment of area of the column, respectively. The results have been obtained from solving the simplified scheme of **Figure 3** by the direct stiffness method.

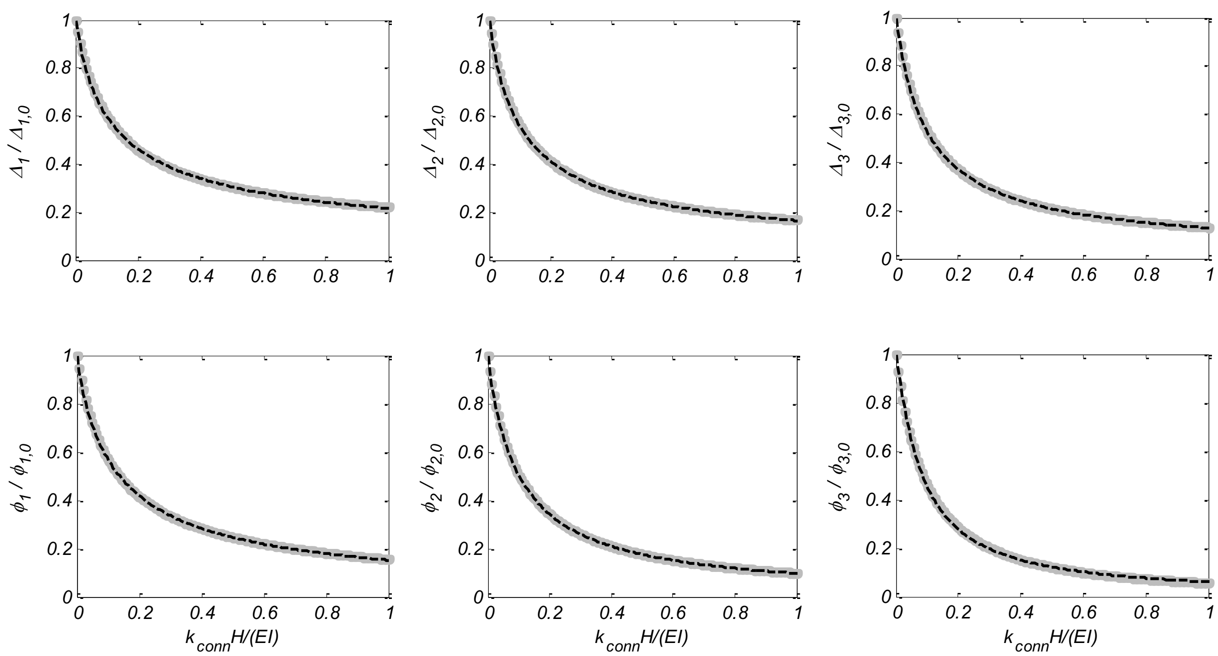


***Figure 5*** *– Parametric analyses assessing the influence of connection stiffness on displacements and rotations*

The dimensionless form allows simplifying the data fitting. The curves shown in **Figure 5** have been fitted by the following equations, whose graphic representation is shown in dashed line in the same figure:

$$\frac{\Delta_{i,conn}}{\Delta_{i,0}} = \frac{l}{\left(\frac{k_{conn} \cdot H}{E \cdot I}\right)^m + l} + n \qquad (8)$$

$$\frac{\varphi_{i,conn}}{\varphi_{i,0}} = \frac{p}{\left(\frac{k_{conn} \cdot H}{E \cdot I}\right)^{q} + p} \tag{9}$$

The coefficients $l$, $m$, $n$, $p$ and $q$ are reported in **Table 2**. All the coefficients have been determined by means of linear least square regression. The analytical expressions of displacements and rotations for the cantilever column ($\Delta_{i,0}$ and $\varphi_{i,0}$) under the lateral load distribution proportional to the first eigenvector (**Figure 4**) are presented in **Table 3**. Such values have been obtained from applying the direct stiffness method.

Therefore, it is possible to obtain column displacements and rotations from the values of the cantilever column case (**Table 3**) directly through **Eq.8** and **Eq.9**.

***Table 2** – Coefficients for **Eq. 8** and **Eq. 9***

| n. Storey | Floor | $l$ | $m$ | $n$ | $p$ | $q$ |
|---|---|---|---|---|---|---|
| 3 | 3 | 0.1194 | 0.9290 | 0.0216 | 0.0643 | 1.1096 |
| | 2 | 0.1510 | 0.8655 | 0.0335 | 0.1081 | 0.9779 |
| | 1 | 0.1989 | 0.7852 | 0.0501 | 0.1792 | 0.8656 |
| 2 | 2 | 0.2510 | 0.8859 | 0.0261 | 0.1499 | 1.0618 |
| | 1 | 0.3439 | 0.7869 | 0.0419 | 0.2649 | 0.9206 |
| 1 | 1 | 0.8966 | 0.7855 | 0.0235 | 0.5 | 1 |

***Table 3** – Displacements and rotations for the cantilever column case according to force distribution in **Figure 4***
*Note: F is the force applied at the roof level*

| n. Storey | Floor | $\Delta$ $\left(\frac{FH^3}{3EI}\right)$ | $\varphi$ $\left(\frac{FH^2}{2EI}\right)$ |
|---|---|---|---|
| 3 | 3 | 35.076 | 11.285 |
| | 2 | 18.649 | 10.285 |
| | 1 | 5.487 | 6.753 |
| 2 | 2 | 8.800 | 4.320 |
| | 1 | 2.820 | 3.320 |
| 1 | 1 | 1 | 1 |

The approximation provided by **Eq.8** and **Eq.9** leads to a maximum error of 5% and 8%, respectively. In the case the inter-storey height of the first floor is 30% higher than the other floors, the maximum errors become 11% and 22%, respectively. In such a case, Eq.8 and Eq.9 are evaluated considering the mean inter-storey height, while the floor displacements are estimated from a linear interpolation of the displacements obtained from the equal inter-storey height case. It is also worth noting that the maximum errors obtained from considering a 50% mass reduction at the roof level are 6% and 11%, respectively; this situation is intended to account for the presence of micro-shed elements and/or skylights on the roof. All the aforementioned errors are referred to $k_{conn}$ $H/(EI)$ less than 1, which is considered an upper bound for the structural typology under investigation.

*Step 3: Capacity curve definition*

The relationship between the lateral loads, displacements and rotations allows defining an approximate capacity curve of the building (**Figure 6**).

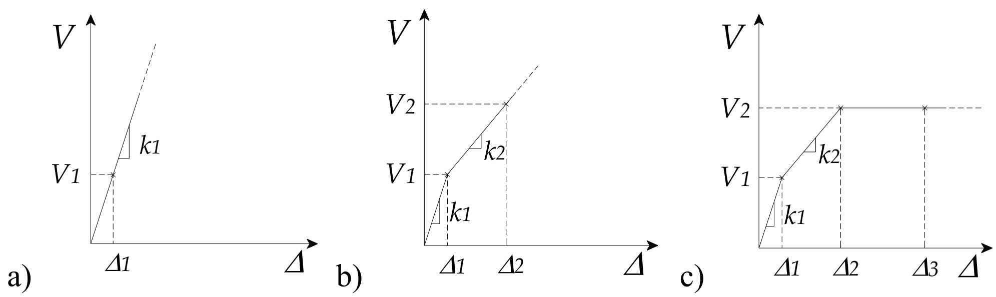


***Figure 6*** *– Approximated capacity curve construction.*
*Note: V is the base shear of the system (sum of horizontal forces $F_i$); Δ is the roof displacement.*

The capacity curve is obtained from the following steps:

a) increase the lateral loads $F_i$ (proportional to the first mode eigenvector, **Figure 4**) until first yielding of the column base or beam-column connection, whichever occurs first. Such condition defines the point ($V_1$, $\Delta_1$);
b) neglect the stiffness of the yielded elements and increase the lateral loads until yielding of the other type of element (beam-column connection or column base). This condition defines the point ($V_2$, $\Delta_2$);
c) keep the base shear constant up to a displacement and rotation corresponding to the failure of an element, following the linear deflected shape of **Figure 7**. The displacements and rotations in **Figure 7** must be added to the corresponding values reached in the previous step (i.e. those corresponding to $V_2$, $\Delta_2$ in **Figure 6**).

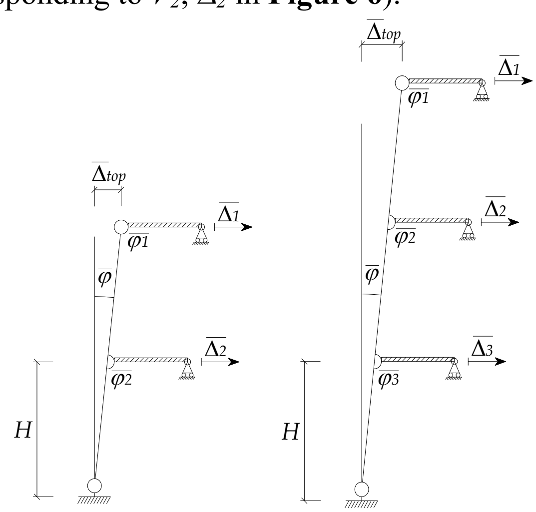


***Figure 7*** *– Rigid rotation of the system corresponding to step c) of the approximated curve definition.*

The capacity curve of the whole system is obtained from summing the contribution of each column. Given the capacity curve, the DBA procedure follows the steps previously described.

## 4. Beam-column connections

The hysteretic behaviour of beam-column connections is obtained from considering an analytical expression for the shear-displacement relationship. In the literature, various formulations are available (CNR 10025, Doneux et al., 2006; Ferreira, 1999; Soroushian et al., 1987, Vintzeleou and Tassios, 1987; Tsoukantas and Tassios, 1989). This paper adopts the formulation proposed by Ferreira (1999) which allows accounting for the pretension of dowels and the presence of an elastomeric bearing.

The considered force-displacement relationship considers three contributions influencing the global deformation of the connection:

a) the deformation of the bar embedded in the concrete (column side);
b) the deformation of the bar embedded in the grout (beam side);
c) the shear deformation of the elastomeric bearing.

The resulting shear-displacement relationship is a tri-linear curve, whose analytical definition is highlighted in the Appendix.

The moment-rotation behaviour of the connection is evaluated for clockwise (**Figure 8a**) or counter-clockwise (**Figure 8b**) bending moments, due to the possible asymmetric position of the dowels in the column corbel and to the possible contact between the top of the beam and the column.

For clockwise bending moment, there is no contact between the top of the beam and the column. A cross-section analysis is conducted considering the cross-section defined by the beam-column interface and a compressive force resulting from the gravity loads and the dowel pretension. The connection failure is associated with either the tension failure of the dowels or bearing failure of the concrete, whichever happens first. If yielding of the dowels in tension happens before the connection failure, the moment-rotation diagram is defined by two points: the first point corresponds to yielding of the dowels, the second point to failure of the connection. The elongation of the dowels at yielding and at failure allows defining the connection rotation.

For counter-clockwise bending moment, the first step considers the evaluation of the failure mode of the connection as in the case of clockwise bending moment. A first estimate of the moment-rotation points is obtained from assuming no contact between the beam and the column. The following step evaluates the effects associated with the contact between the top of the beam and the column. Three situations are possible:

a) the contact is reached before yielding of the dowels;
b) the contact is reached before connection failure;
c) no contact until connection failure.

The moment-rotation diagram evaluated in the first step (i.e. considering no contact between the beam and the column) is valid only for rotations smaller than the contact rotation. After beam-column contact, the connection is subjected to a stiffness increase. The post-contact bending moment is obtained from the product of the shear resistance of the connection (i.e. from the force-displacement curve) and the resulting lever arm, herein assumed equal to 0.9h. After shear failure of the connection, the beam can still rotate with a bending moment given by the product of the concrete-neoprene friction force and the lever arm. Such condition is not considered herein due to the uncertainty in the response, as for instance related to the influence of the vertical component of the earthquake. The Appendix contains a calculation example for the aforementioned formulation.

In the present paper, the moment-rotation and force-displacement relationship of the beam-column connections are directly included in the finite element models by means of one rotational spring and one translational spring, respectively. **Figure 9** shows a possible modelling strategy able to account for the coupled translational-rotational behaviour of beam-column connections.

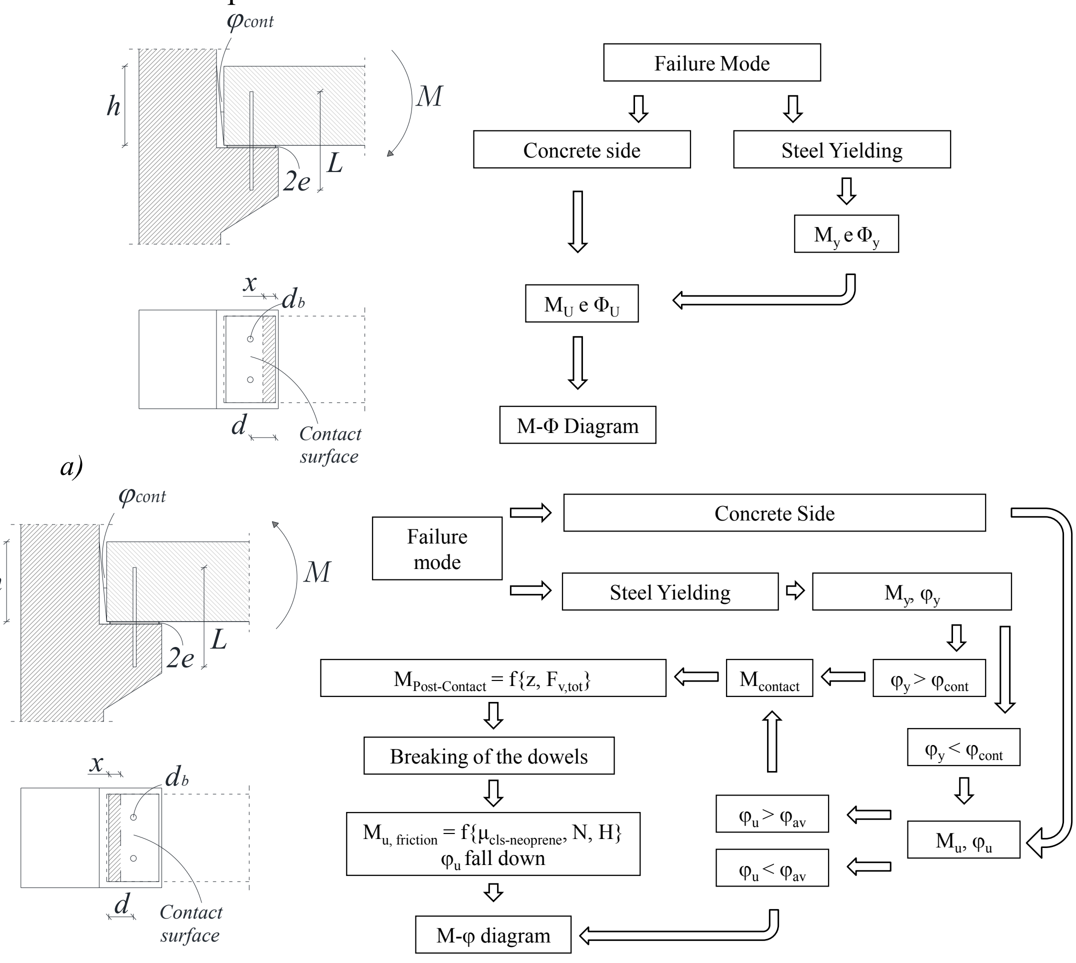


***Figure 8*** *– Beam-column connection behaviour:*
*a) clockwise bending moment; b) counter-clockwise bending moment.*

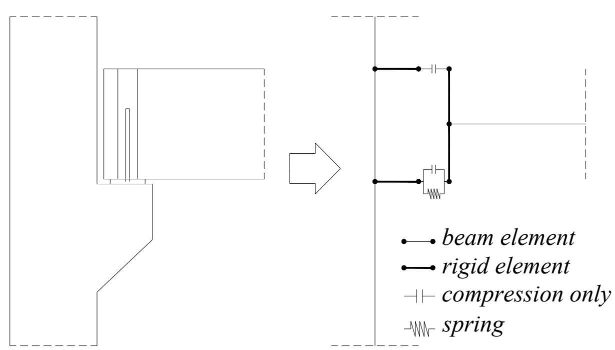


***Figure 9*** *– Alternative modelling scheme for beam-column connections.*

## 5. P-Δ effects

During an earthquake, second order P-Δ effects could significantly increase the horizontal displacements achieved by a structure and therefore need to be accounted for in a seismic assessment procedure. The methodology proposed in Belleri et al. (2017a) is considered herein. Such procedure is briefly summarized in the following.
In the first step, the capacity curve is reduced to account for second order effects (**Figure 10**). The bilinearization of the capacity curve needs to allow for negative post-yield stiffness.

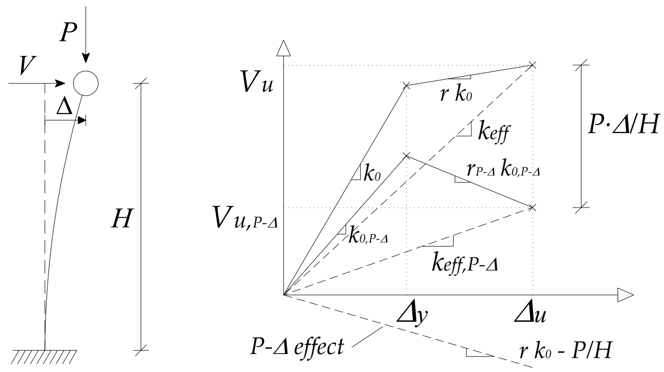


***Figure 10** – Influence of P-Δ effects on the structural response of a SDOF system*

In the second step the EVD of the equivalent SDOF system is adjusted. It is worth mentioning that the available EVD formulations (as for instance Grant et al. 2004, Priestley et al. 2007) have been calibrated based on the force-displacement response of inelastic SDOF systems with positive post yield stiffness ratio ($r$), typically $r = 0.05$. Therefore, given $\Delta_u$, the actual SDOF system response considering P-Δ effects is represented by Curve A in **Figure 11**, while the actual curve considered in the EVD formulation is represented by Curve B, leading to a net hysteretic energy underestimation and consequently EVD underestimation. It is worth noting that to account for P-Δ effects in the DBD procedure, Priestley et al. (2007) recommended to adjust the base-shear with a specific coefficient which depends on the hysteretic system but also on the main characteristics of the ground motions. Indeed, the hysteretic energy that might be underestimated is offset by dynamic ratcheting that is more significant for non-linear systems with high P-Δ loads (Priestley et al., 2007).

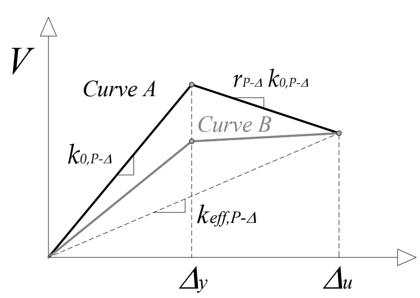


***Figure 11** – Curve A: SDOF response including P-Δ effects; Curve B: SDOF response used in EVD formulation*

Herein, **Eq.7** is modified by means of a correction factor (λ) to account for differences in the hysteretic energy estimation:

$$\eta_{P-\Delta} = \sqrt{0.10 / \left(0.05 + \lambda \cdot \xi_{eq\ r=0.05}\right)} \tag{10}$$

Where $\eta_{P\text{-}\Delta}$ represents the ratio between the damped displacement spectrum including P-Δ effects (EVD = $\lambda \cdot \xi_{eq\ \ r=0.05}$) and the elastic displacement spectrum (EVD = 0.05). For the considered structural typology, λ is:

$$\lambda\left(r_{P-\Delta}, \mu_\Delta\right) = \left(4.57 \cdot \mu_\Delta - 5.53\right)\left(r_{P-\Delta}{}^2 - 0.0025\right) - \left(1.19 \cdot \mu_\Delta - 0.80\right)\left(r_{P-\Delta} - 0.05\right) + 1 \tag{11}$$

The correction factor $\lambda$ has been derived from a parametric analysis considering different values of post-yield stiffness ratio, system ductility and effective period. A series of non-linear dynamic analyses of SDOF systems allowed the calibration of the coefficients of **Eq.11** by means of non-linear regression analyses (Belleri et al., 2017a).

## 6. Influence of the second mode of vibration

The beam-column connection is a critical detail of existing precast structures. Therefore, the seismic demand in terms of connection rotation must be carefully evaluated. The displacement profile considered in the DBA procedure is obtained from the PM or ECSM method. In both approaches, the target limit state is evaluated from a force distribution proportional to the first mode of vibration, not accounting for higher modes of vibration. This could lead to possible underestimation of the connection rotation demand.
Various methods have been developed to consider the influence of higher modes of vibration in non-linear static analyses, such as the Modal Pushover Analysis developed by Chopra and Goel (2002) and the extended N2 method proposed by Kreslin and Fajfar (2011). In the framework of displacement based design, Priestley et al. (2007) proposed a method to predict the shear force and moment envelopes in the structural elements accounting for higher modes of vibration. This method, known as modified modal superposition (MMS), considers a modal combination (such as the square root of the sum of squares, SRSS) in which the shear and moment distribution of the first mode are taken from the displacement based design procedure and the corresponding distribution of the higher modes are taken form an elastic response spectrum analysis. Sullivan et al. (2008) highlighted the influence of higher modes in ductile structures.
The method considered herein is an extension of MMS for the assessment of existing structures. The proposed approach is based on the following assumptions:

- i. the first mode of vibration is the predominant mode in terms of inelastic displacement distribution;
- ii. only the influence of the second mode of vibration is considered to refine the results obtained from the DBA procedure;
- iii. all the hysteretic energy dissipation is associated with the first mode of vibration; the second mode is considered elastic.

The procedure is described in the following steps.

*Step 1: Application of the DBA procedure*

The DBA procedure is applied to the structure, considering the inelastic displacement profile obtained from a force distribution proportional to the first mode of vibration. The DBA procedure allows the definition of the peak ground acceleration associated with the first mode of vibration (*PGA $1^{st}$mode*). The corresponding forces/deformations are recorded as $R_1$.

*Step 2: Elastic response spectrum of the 2nd mode of vibration*

The influence of the 2nd mode of vibration is evaluated by means of an elastic modal analysis accounting for the sole second mode. The *PGA 1st mode* (Step 1) allows defining the elastic spectrum (ξ=5%) used to identify the spectral acceleration ($S_{e,2nd\ mode}$) associated with the second mode of vibration ($T_{2nd\ mode}$ in **Figure 12**). The modal analysis is performed placing elastic rotational springs at the beam-column connections and at the column base; for this the secant stiffness for each connection is considered. The secant stiffness is calculated as the ratio between the flexural moment and the rotation associated with the considered limit state.

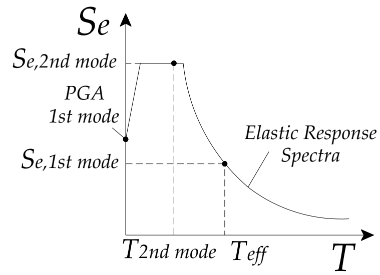


***Figure 12*** *– Evaluation of the spectral acceleration of the second mode of vibration ($S_{e,2nd\ mode}$).*

The effects in terms of forces/deformations obtained from the modal analysis are combined following the SRSS rule with the results of Step 1 ($R_1$). The combined results are referred to as $R_2$.

*Step 3: Definition of a correction factor*

A correction factor $c_f$ is defined:

$$c_f = R_{1,c} / R_{2,c} \tag{12}$$

$R_{1,c}$ and $R_{2,c}$ are the deformations/forces for the critical element obtained from Step 1 and Step 2, respectively; the critical element is the element associated with the definition of the target limit state. The target displacement $\Delta_u$ defined in the DBA procedure is reduced by the correction factor $c_f$; the new target displacement ($\Delta_{u,2}$) is

$$\Delta_{u,2} = c_f \cdot \Delta_u \tag{13}$$

*Step 4: DBA procedure including 2nd mode effects*

The properties of the equivalent structure are redefined according to $\Delta_{u,2}$ and a new point associated with the target limit state ($V_{u,2}$, $\Delta_{u,se2}$) is estimated following the DBA procedure. Iterations between Step 1 and Step 4 may be required until convergence.
It is worth noting that only the second mode of vibration is considered herein. The contributions of other relevant modes of vibration could be included in a similar way.

## 7. DBA procedure for selected case studies

The proposed DBA procedure is validated considering two planar frames (Case Study A and Case Study B) representative of three-storey precast buildings. The seismic vulnerability is evaluated in terms of the peak ground acceleration on rock ($a_g$) associated with the target limit state. The proposed seismic assessment methods (DBA-ECSM and DBA-PM) are considered and compared to the results obtained from non-linear dynamic analyses (Incremental Dynamic Analyses, IDA).

Figure 11 shows the geometry for Case Study A. The frame is composed by 6 beams with rectangular cross section (300x500 mm), 3 columns with a total height equal to 9 m and square cross section (350x350 mm). The concrete compressive strength is 50 MPa, while the grout surrounding the dowels has a compressive strength of 59 MPa. The steel yield strengths are 480 MPa and 340 MPa for the column rebars and the connection dowels, respectively. The column longitudinal reinforcement is made by 8 rebars (24mm diameter). The resulting bending moment capacity is 327 kNm considering an axial load equal to 472 kN. The beam-column connection is made of two dowels (12mm diameter) with a supporting neoprene cushion (5 mm thick) (**Figure 13**). A seismic mass equal to 75,000 kg is considered at each floor of the frame. Soil-structure interaction is not accounted for and the columns are assumed fixed to the ground. Regarding EVD, the contribution of the beam-column connection has been neglected herein, due to the low dissipation capacity of the connection compared to the plastic hinge at the column base. Case Study B differs from Case Study A in that the column cross-section is bigger (600x600mm,) and the stiffness of the beam-column connection is 4 times higher than Case Study A. The column longitudinal reinforcement is made by 16 rebars (18mm diameter) which leads to a bending moment capacity equal to 1005 kNm.

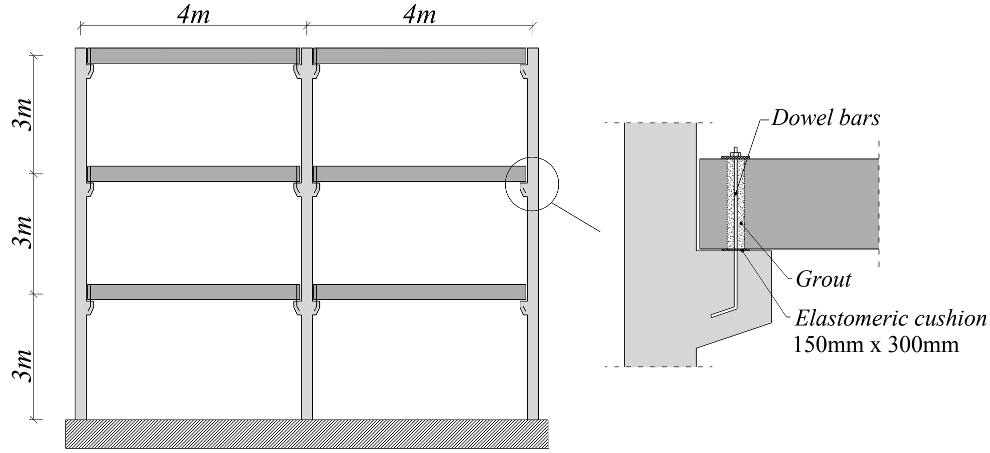


***Figure 13** – Geometry of the considered frame.*

## *7.1 DBA with the Equivalent Column Simplified Method (DBA-ECSM)*

The capacity curve is obtained from following the ECSM method. First, the displacements and rotations of the cantilever column are calculated from **Table 3** following an arbitrary lateral load distribution proportional to the first mode of vibration (**Figure 4**). Such arbitrary loads (25.0 kN, 13.3 kN and 3.9 kN for 3$^{rd}$, 2$^{nd}$, and 1$^{st}$ floor, respectively) allow defining the initial elastic branch of the capacity curve.

Considering a beam-column connection stiffness ($k_{conn}$) equal to 2480 kNm/rad and 10000 kNm/rad for Case Study A and Case Study B respectively, the resulting values of the ratio

$k_{conn}/(EI/H)$ are 0.159 and 0.074, respectively. The column lateral displacements and rotations accounting for the beam-column connection stiffness (**Table 4**) are obtained from **Eq.8** and **Eq.9**.

***Table 4*** *– Displacements and rotations for the cantilever case with and without beam-column connections*

| | Case study A | | | | Case study B | | | |
|---|---|---|---|---|---|---|---|---|
| Storey | $\Delta_{i,0}$ (mm) | $\Delta_{i,conn}/\Delta_{i,0}$ | $\varphi_{i,0}$ (rad) | $\varphi_{i,conn}/\varphi_{i,0}$ | $\Delta_{i,0}$ (mm) | $\Delta_{i,conn}/\Delta_{i,0}$ | $\varphi_{i,0}$ (rad) | $\varphi_{i,conn}/\varphi_{i,0}$ |
| 3 | 168.7 | 43.0% | 0.0271 | 34.3% | 19.5 | 60.8% | 0.0031 | 55.2% |
| 2 | 89.7 | 47.4% | 0.0247 | 40.6% | 10.4 | 64.5% | 0.0029 | 58.8% |
| 1 | 26.4 | 52.7% | 0.0162 | 48.5% | 3.1 | 69.2% | 0.0019 | 65.1% |

The lateral loads are then increased until failure of the first connection. The second branch of the capacity curve is obtained from considering a residual stiffness of the system equal to the column stiffness without beam-column connections. The lateral loads are further increased until yielding of the column base. The last branch of the curve is obtained increasing displacements and rotations linearly until failure of the first connection or until a selected limit state. Table 5 shows the results of such procedure. **Figure 14** shows the resulting capacity curve.

***Table 5*** *– Main data of the DBA-ECSM procedure.*
*(*) failure of the connections for Case Study A and of the column base for Case Study B*

| | | Yielding of connection | | | Yielding of column base | | | Failure | | |
|---|---|---|---|---|---|---|---|---|---|---|
| Case Study | Storey | $\Delta_{i,conn}$ (mm) | $\varphi_{i,conn}$ (rad) | $F_i$ (kN) | $\Delta_{i,conn}$ (mm) | $\varphi_{i,conn}$ (rad) | $F_i$ (kN) | $\Delta_{i,conn}$ (mm) | $\varphi_{i,conn}$ (rad) | $F_i$ (kN) |
| A | 3 | 18.2 | 0.0023 | 6.3 | 163.4 | 0.0257 | 27.8 | 314.9 | 0.0425 | 27.8 |
| | 2 | 10.7 | 0.0025 | 3.3 | 87.9 | 0.0238 | 14.8 | 188.9 | 0.0406 | 14.8 |
| | 1 | 3.5 | 0.0020 | 1.0 | 26.2 | 0.0159 | 4.4 | 76.7 | 0.0328 | 4.4 |
| B | 3 | 4.3 | 0.0006 | 9.0 | 61.3 | 0.0098 | 82.0 | 287.6 | 0.0349 | 82.0 |
| | 2 | 2.4 | 0.0006 | 4.9 | 32.7 | 0.0090 | 43.6 | 183.9 | 0.0341 | 43.6 |
| | 1 | 0.8 | 0.0004 | 1.4 | 9.7 | 0.0059 | 12.9 | 85.1 | 0.0311 | 12.9 |

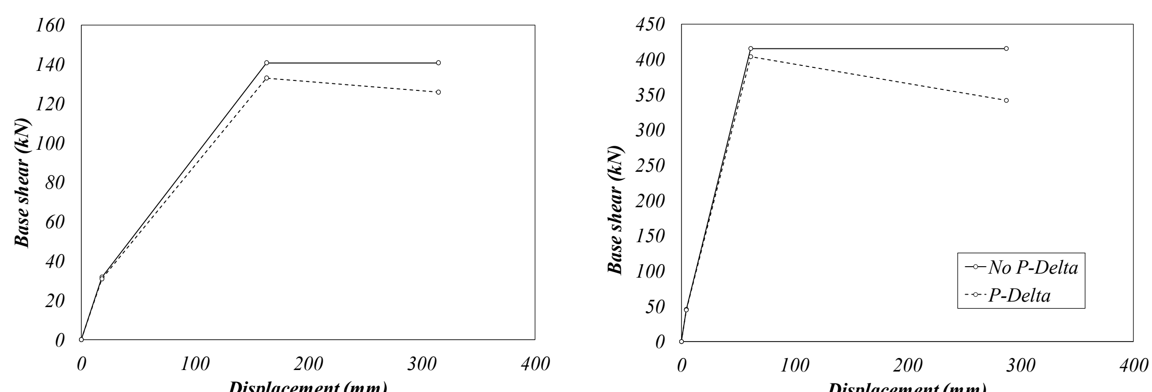


a) b)

*Figure 14* – *DBA-ECSM capacity curve: a) Case Study A; b) Case Study B*

The capacity curve is bilinearized and the yield and target displacements corresponding to the considered limit states are calculated. This allows defining the equivalent SDOF system (**Table 1**). **Table 5** shows the properties of the equivalent SDOF system and the results of the DBA-ECSM procedure in terms of $a_g$.

***Table 5*** *– DBA-ECSM: equivalent SDOF system properties and results*

| | Case Study A | | Case Study B | |
|---|---|---|---|---|
| | No P-Δ | P-Δ | No P-Δ | P-Δ |
| $\Delta_{y,\,SDOF}$ (mm) | 114.0 | 114.0 | 46.0 | 46.0 |
| $V_{y,\,SDOF}$ (kN) | 142.0 | 134.6 | 416.4 | 405.2 |
| $\Delta_{u,\,SDOF}$ (mm) | 243.8 | 245.6 | 222.7 | 222.9 |
| $V_{u,\,SDOF}$ (kN) | 140.8 | 125.9 | 415.5 | 341.9 |
| $EVD_{r=0.05}$ (%) | 15.76 | 15.83 | 21.04 | 21.05 |
| $k_{eff}$ (kN/mm) | 577.6 | 512.6 | 1866.0 | 1534.1 |
| $m_{eff}$ (kN/g) | 177.3 | 177.3 | 187.4 | 187.4 |
| $T_{eff}$ (sec) | 3.48 | 3.70 | 1.99 | 2.19 |
| η | 0.69 | 0.65 | 0.62 | 0.54 |
| $a_g$ (g) | 0.410 | 0.438 | 0.421 | 0.486 |

*7.2 DBA with the Pushover Method (DBA-PM)*

The inelastic deflected shape of the system is obtained from a pushover analysis, similarly to typical non-linear static analyses. **Figure 15** shows the resulting capacity curves. The properties of the equivalent SDOF structure are evaluated according to the aforementioned DBA procedure and reported in **Table 4** along with the results of the DBA-PM procedure in terms of $a_g$.

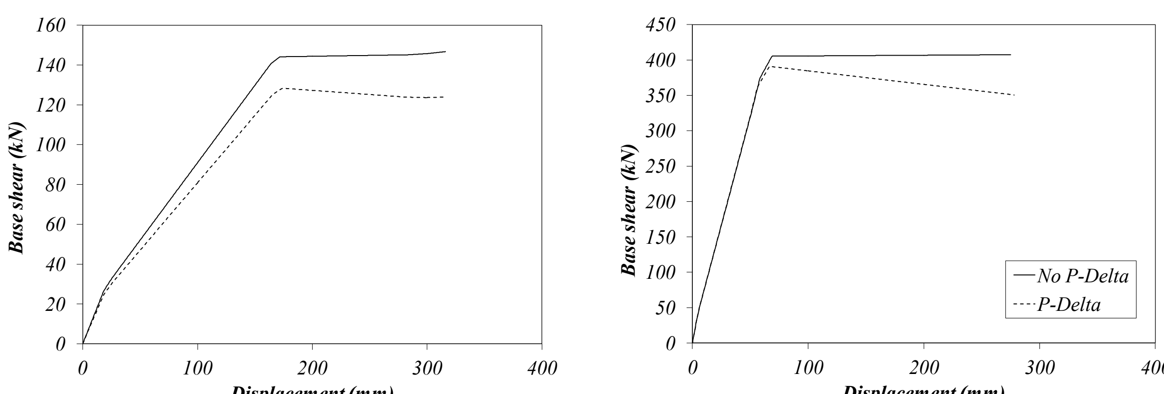


a) b)

*Figure 15* – *DBA-PM capacity curve: a) Case Study A; b) Case Study B*

***Table 6*** *– DBA-PM: equivalent SDOF system properties and results*

| | Case study A | | Case study B | |
|---|---|---|---|---|
| | No P-Δ | P-Δ | No P-Δ | P-Δ |
| $\Delta_{y,\,SDOF}$ (mm) | 121.7 | 122.4 | 49.6 | 44.8 |
| $V_{y,\,SDOF}$ (kN) | 144.4 | 129.5 | 404.4 | 391.2 |
| $\Delta_{u,\,SDOF}$ (mm) | 243.1 | 242.6 | 214.6 | 216.1 |
| $V_{u,\,SDOF}$ (kN) | 146.7 | 123.9 | 407.5 | 350.6 |
| $EVD_{r=0.05}$ (%) | 15.10 | 15.01 | 20.55 | 21.03 |
| $k_{eff}$ (kN/mm) | 603.5 | 510.8 | 1898.5 | 1622.8 |
| $m_{eff}$ (kN/g) | 179.5 | 178.7 | 187.0 | 187.1 |
| $T_{eff}$ (sec) | 3.43 | 3.72 | 1.97 | 2.13 |
| $\eta$ | 0.70 | 0.67 | 0.63 | 0.55 |
| $a_g$ (g) | 0.402 | 0.421 | 0.406 | 0.462 |

### *7.3 Validation by means of Incremental Dynamic Analyses (IDA)*

Non-linear time history analyses have been carried out to validate the investigated DBA procedure. In particular, Incremental Dynamic Analyses have been conducted. The $a_g$ values associated with the target limit states are estimated as the mean value of the results of time history analyses under 14 ground motions. The earthquake records[2] have been selected from the European strong-motion database (Ambraseys et al. 2002) in such a way to be spectrum compatible in displacement with EN 1998-1 type 1 spectrum ($a_g=0.300g$, $S=1.15$, $T_B=0.2$, $T_C=0.6$, $T_D=2$). **Figure 16** shows the displacement response spectrum of each record (GM), the resulting mean spectrum and the target spectrum.

The ground motion set has been incrementally scaled (i.e. the same additional scale factor is applied to each ground motion) to achieve the target limit state in the non-linear time history analyses. The selected limit state corresponds to the first collapse of a beam-column connection for Case Study A and to flexural failure of the base column for Case Study B. **Table 7** shows the results of the analyses in terms of $a_g$.

***Table 7*** *– IDA results*

| | Limit state | $a_{g\_IDA}$ (No P-Δ) (g) | $a_{g\_IDA}$ (P-Δ) (g) |
|---|---|---|---|
| Case Study A | Failure of beam-column connection | 0.398 | 0.393 |
| Case Study B | Flexural failure at column base | 0.491 | 0.480 |

[2] Waveform id according to Ambraseys et al. (2004). Scale factor in brackets.
000343xa (1.250), 000244xa (1.455), 000472xa (0.978), 000302ya (1.565), 000644xa (0.867), 000359xa (1.470), 000707ya (1.182), 000377ya (1.428), 001769ya (1.234), 005270xa (1.519), 001769ya (1.234), 005791ya (1.518), 006960ya (0.827), 005815xa (1.484)

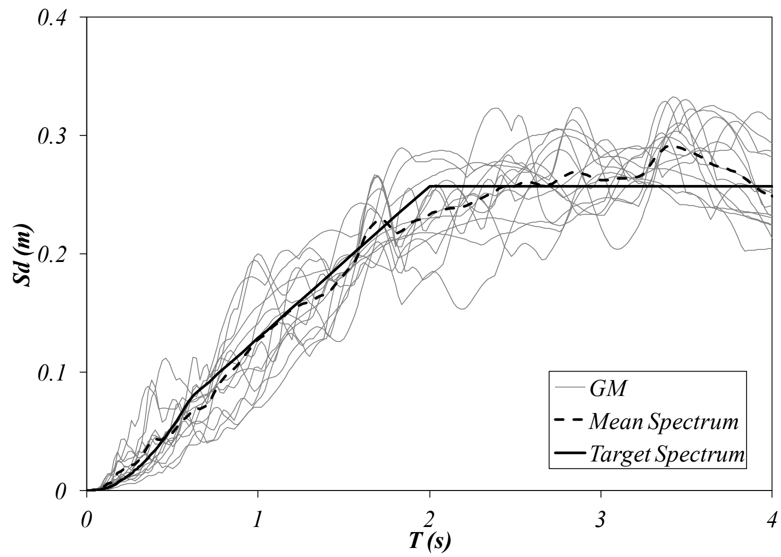


***Figure 16** – Displacement spectrum of the selected ground motions.*

**Table 8** shows the comparison of the investigated DBA methods in dimensionless terms through the ratio between the DBA results ($a_g$) and the IDA results ($a_{g\_IDA}$). Both DBA methods provide relatively good estimations, with a maximum error equal to 17% and 12% for Case Study B and A, respectively. It is worth noting that, for the considered case studies, DBA-ECSM leads to quite similar results compared to DBA-PM. In addition, a maximum 16% difference was recorded for ECSM when the influence of the second mode of vibration was not considered.

***Table 8** – Results comparison: $a_g/a_{g\_IDA}$*

| | Case study A | | Case study B | |
|---|---|---|---|---|
| | No P-Δ | P-Δ | No P-Δ | P-Δ |
| DBA – PM | 1.01 | 1.07 | 0.83 | 0.96 |
| DBA – ECSM | 1.03 | 1.12 | 0.86 | 1.01 |

## 8. Conclusions

The paper presents a Displacement Based Assessment (DBA) methodology for the evaluation of the seismic vulnerability of existing precast frame structures. The procedure specifically relates the seismic assessment to the building lateral displacements. Considering the high deformability of precast buildings, combined with the high deformation demand in the beam-column connections, the displacement is a suitable seismic vulnerability indicator. Furthermore, the non-linearity of the system is directly accounted for by the equivalent viscous damping, without requiring the definition of a behaviour factor as in standard linear methods.

The proposed procedure follows the same framework developed in the Direct Displacement Based Design methodology and it can be applied in a different sequence of steps compared to what presented in the paper, to suit the engineer or structure in question, without affecting the core principles of the approach. The definition of the inelastic displacement profile is the major difficulty in the development of the method, since the non-linear behaviour of the elements, particularly beam-column connections, strongly affects the displacement distribution along the building height. Two different solutions are proposed: the Pushover based Method (PM) and the Equivalent Column Simplified Method (ECSM). Both approaches allow the definition of the inelastic displacement profile, considering the non-linearity associated with structural elements and connections, although ECSM is based on a simplified definition of the displacement profile which can be implemented in spreadsheets.

The procedure is further refined including the influence of P-Δ effects and of the second mode of vibration of the structure. P-Δ effects are accounted for by modifying the equivalent viscous damping of the equivalent SDOF system. The second mode of vibration may be considered by introducing the corresponding elastic forces combined with the forces associated with the first mode of vibration. If the second mode of vibration is neglected, the assessment procedure may underestimate the rotation of beam-column connections.

The proposed procedure has been validated by means of non-linear time history analyses (incremental dynamic analyses). Two case studies have been selected resembling 3-storey precast concrete frames. The DBA provides an approximate estimate of the building response if compared to the results of incremental dynamic analyses: the maximum errors are 17% and 12% for Case Study A and B, respectively. Finally, it is worth noting that, for the considered case studies, DBA-ECSM leads to quite similar results compared to DBA-PM, therefore providing a useful assessment tool for a first estimate of the seismic vulnerability.

**Funding**

The financial support of the Italian Reluis project (“Programma Quadro DPC-Reluis 2010-2013 - Sviluppo di approcci agli spostamenti per la valutazione della vulnerabilità”) is greatly acknowledged.

**Acknowledgements**

The authors sincerely thank the anonymous reviewers for the fruitful comments provided. The opinions and findings are those of the authors and do not necessarily reflect the view of the people and the organization acknowledged.

## References


Ambraseys N., Smit P., Sigbjornsson R., Suhadolc P., Margaris B. (2002) Internet-Site for European Strong-Motion Data, European Commission, Research-Directorate General, Environment and Climate Programme

ASCE/SEI 41 (2014), Seismic evaluation and retrofit of existing buildings, American Society of Civil Engineers, Reston, Virginia, USA

Belleri A., Torquati M., Riva P. (2014) Seismic performance of ductile connections between precast beams and roof elements. Magazine of Concrete Research, 66(11):553-562

Belleri A., Brunesi E., Nascimbene R., Pagani M., Riva P. (2015a) Seismic Performance of Precast Industrial Facilities Following Major Earthquakes in the Italian Territory. J. Perform. Constr. Facil., 29(5):04014137.

Belleri A., Torquati M., Riva P., Nascimbene R. (2015b) Vulnerability assessment and retrofit solutions of precast industrial structures. Earthquake and Structures, 8(3):801-820

Belleri A., Torquati M., Marini A., Riva P. (2016) Horizontal cladding panels: in-plane seismic performance in precast concrete buildings. Bulletin of Earthquake Engineering, 14(4):1103-1129

Belleri A., Torquati M., Marini A., Riva P. (2017a) A Novel Framework to Include P-Δ Effects in Displacement-Based Seismic Assessment. Journal of Earthquake Engineering, 21(3):486-492

Belleri A. (2017b) Displacement based design for precast concrete frames with non-emulative connections. Engineering Structures, 141:228-240

Brunesi E., Nascimbene R., Bolognini D., Bellotti D. (2015) Experimental investigation of the cyclic response of reinforced precast concrete framed structures. PCI Journal, 15(2):57-79

Cardone D. (2014) Displacement limits and performance displacement profiles in support of direct displacement-based seismic assessment of bridges. Earthquake Engineering and Structural Dynamics, 43: 1239–1263

Casotto C., Silva V., Crowley H., Nascimbene R., Pinho R. (2015) Seismic Fragility of Italian RC Precast Industrial Structures. Engineering Structures, 94:122-136

Chopra A.K., Goel R.K. (2002) A modal pushover analysis procedure for estimating seismic demands for buildings. Earthquake Engineering and Structural Dynamics, 31:561–582

Clementi F., Scalbi A., Lenci S. (2016) Seismic performance of precast reinforced concrete buildings with dowel pin connections. Journal of Building Engineering, 7:224-238

CNR 10025 (1984) Istruzioni per il progetto, l'esecuzione e il controllo delle strutture prefabbricate in conglomerato cementizio e per le strutture costruite con sistemi industrializzati, Roma, Italy

Crisafulli F., Carr A. (2007) Porposed macro-model for the analysis of infilled frame structures. Bulletin of New Zealand Society for Earthquake Engineering, 40:69–77

Doneux C., Hausoul N., Plumier A. (2006) Analysis of 3 precast RC structures with dissipative connections. In Risk mitigation for Earthquake and Landslides Integrated Project, Project No.: GOCE-CT-2003-505488, Sub-Project 2.2b.6.2 – Upgrading of precast concrete structures by energy dissipative connections, pp. 60-75

Dwairi H.M., Kowalsky M.J., Nau J.M. (2007) Equivalent Damping in Support of Direct Displacement-Based Design. Journal of Earthquake Engineering, 11:512-530

El-Dakhakhni W.W., Elgaaly M., Hamid A.A. (2003) Three-strut model for concrete masonry-infilled steel frames. Journal of Structural Engineering, 129:177–185

EN 1998-1:2005, Eurocode 8: Design of structures for earthquake resistance - Part 1: General rules, seismic actions and rules for buildings, European Committee for Standardization, Brussels, Belgium

Ercolino M., Magliulo G., Manfredi G. (2016) Failure of a precast RC building due to Emilia-Romagna earthquakes. Engineering Structures, 118:262-273

Fajfar P., Dolsek M. (2010) A practice-oriented approach for probabilistic seismic assessment of building structures. In Advances in Performance-Based Earthquake Engineering, M.N. Fardis editor, pp 225-233

Ferreira M.A. (1999) Deformability of beam-column connections in precast concrete structures. PhD Thesis – School Engineering of São Carlos, University of São Paulo at São Carlo

FEMA 154 (2002) Rapid Visual Screening of Buildings for Potential Seismic Hazards: A Handbook, Second Edition, Washington DC, USA

Grant D.N., Blandon C.A., Priestley M.J.N. (2004) Modelling Inelastic Response in Direct Displacement-Based Design. IUSS Press, Pavia, Italia

Kremmyda G.D., Fahjan Y.M., Psycharis I.N., Tsoukantas S.G. (2017) Numerical investigation of the resistance of precast RC pinned beam-to-column connections under shear loading. Earthquake Engineering and Structural Dynamics, 46:1511-1529

Kreslin M., Fajfar P., (2011) The extended N2 method taking into account higher mode effects in elevation. Earthquake Engineering and Structural Dynamics, 40:1571–1589

Landi L., Tardini A., Diotallevi P.P. (2016) A Procedure for the Displacement-Based Seismic Assessment of Infilled RC Frames. Journal of Earthquake Engineering, 20(7):1077-1103

Magliulo G., Ercolino M., Cimmino M., Capozzi V., Manfredi G. (2015) Cyclic shear test on a dowel beam-to-column connection of precast buildings. Eartquakes and Structures an International Journal, 9(3):541-563

Magliulo G., Ercolino M., Petrone C., Coppola O., Manfredi G., (2013) Emilia Earthquake: the Seismic Performance of Precast RC Buildings. Earthquake Spectra, 30(2):891-912

Minghini F., Ongaretto E., Ligabue V., Savoia M., Tullini N. (2016) Observational failure analysis of precast buildings after the 2012 Emilia earthquakes. Earthquake and Structures, 11(2):327-346

Otani S. (1974) SAKE: A Computer Program for Inelastic Response of R/C Frames to Earthquakes. Civil Engineering Studies SRS-413, University of Illinois at Urbana-Champaign, 11/1974

Palanci M., Senel S.M., Kalkan A. (2017) Assessment of one story existing precast industrial buildings in Turkey based on fragility curves, Bulletin of Earthquake Engineering, 15(1):271-289

Pennucci D., Calvi G.M., Sullivan T.J. (2011) Displacement reduction factors for the design of medium and long period structures. Journal of Earthquake Engineering, 15(sup1):1-29

Priestley M.J.N. (1997). "Displacement-based seismic assessment of reinforced concrete buildings". Journal of Earthquake Engineering, Vol. 1 N.1, 157-192

Priestley M.J.N., Calvi G.M., Kowalsky M.J. (2007) Displacement-Based seismic design of structures, IUSS Press, Pavia, Italy

Scotta R., De Stefani L., Vitaliani R. (2015) Passive control of precast building response using cladding panels as dissipative shear walls. Bulletin of Earthquake Engineering 13(11):3527-3552

Soroushian P., Obaseki K., Rojas M., Najm H.S. (1987) Behavior of bars in dowel action against concrete cover. ACI Structural Journal, 84(S18):170-176

Sullivan T.J., Calvi G.M. (2013) Developments in the Field of Displacement-Based Seismic Assessment. Research Report Rose 2013/01, IUSS Press, Pavia, Italy

Sullivan T.J., Priestley M.J.N., Calvi G.M. (2008) Estimating the Higher-Mode Response of Ductile Structures. Journal Of Earthquake Engineering, 12(3):456-472

Rodrigues H., Varum H., Costa A. (2010) Simplified macro-model for infill masonry panels. Journal of Earthquake Engineering, 14:390–416

Toniolo G., Colombo A., (2012) Precast concrete structures: the lessons learned from the L'Aquila earthquake. Structural Concrete 13:73-83

Toniolo G., Dal Lago B. (2017) Conceptual design and full-scale experimentation of cladding panel connection systems of precast buildings. Earthquake Engineering and Structural Dynamics, 46: 2565–2586

Tsoukantas S.G., Tassios T.P. (1989) Shear resistance of connections between reinforced concrete linear precast elements. ACI Structural Journal, 86(S26):242- 249

Vintzeleou E.N., Tassios T.P. (1987) Behavior of Dowels under Cyclic Deformation. ACI Structural Journal. 84(S3):18-30

Welch D.P., Sullivan T.J., Calvi G.M. (2014) Developing Direct Displacement-Based Procedures for Simplified Loss Assessment in Performance- Based Earthquake Engineering. Journal of Earthquake Engineering, 18(2):290-322

Zoubek B., Isakovic T., Fahjan Y., Fischinger M. (2013) Cyclic failure analysis of the beam-to-column dowel connections in precast industrial buildings. Engineering Structures, 52:179-191

Zoubek B., Fischinger M., Isakovic T. (2016) Cyclic response of hammer-head strap cladding-to-structure connections used in RC precast building. Engineering Structures, 119:135-148

## Appendix

In this section, the shear-displacement relationship of dowel beam-column connections is presented following the formulation proposed by Ferreira (1999). A tri-linear force-displacement curve is obtained from defining the connection yielding, the maximum shear capacity of the dowels and the ultimate displacement. **Figure A1** shows the curve whose main points will be described later. The procedure is applied to the beam-column connection of Case Study A (properties shown in **Table A1**).

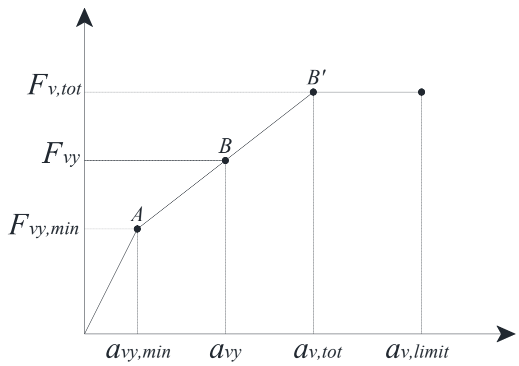


Where:

$$a_{vy,\min} = \lambda_{\tau,lig} \cdot F_{vy,\min}$$

$$a_{vy} = \alpha_{crit} \cdot l_p = \alpha_{crit} \cdot \left(x_1 + x_2 + h_n\right)$$

B' = extrapolated from line A-B

***Figure A1*** *– Force-displacement relationship for dowel connections.*

***Table A1*** *– Properties of the beam-column connection of Case Study A*

| Geometry | Concrete and grout | Neoprene | Dowels |
|---|---|---|---|
| Beam section: 30x50 cm | Concrete compressive strength $f_{ck,min}$ = 40 MPa | Plan geometry: 30x15 cm | Tensile strength: $f_{yk}$ = 340 MPa |
| Gap between beam and column: *gap* = 2 cm | Grout compressive strength $f_{ck,max}$ = 59 MPa | thickness: $h_n$ = 0.5 cm | Number of dowels: $n$ = 2 |
| Length of the corbel $L$ = 40 cm | | shear modulus: $G_{neo}$ = 1 MPa | Diameter: $d_b$ = 12 mm |

The procedure assumes that the post-tension of the dowels leads to a reduced steel strength ($f_{sy,red}$):

$$f_{sy,red} = 0.7 \cdot f_{y,k} = 0.70 \cdot 340 = 238 \ MPa \tag{A.1}$$

The relative stiffness coefficient (Ferreira 1999) of the dowels embedded in the concrete and in the grout are calculated, respectively $k_{c,min}$ and $k_{c,max}$:

$$k_{c,\min} = 127 \cdot \frac{\sqrt{f_{ck,\min}}}{d_b^{2/3}} = 127 \frac{\sqrt{40}}{12^{2/3}} = 153.24 \ MPa/mm \tag{A.2}$$

$$k_{c,\max} = 127 \cdot \frac{\sqrt{f_{ck,\max}}}{d_b^{2/3}} = 127 \frac{\sqrt{59}}{12^{2/3}} = 186.11 \ MPa/mm \tag{A.3}$$

The following parameters are calculated according to the theory of a beam resting on an elastic foundation:

$$\alpha_{\min} = \sqrt[4]{\frac{k_{c,\min} \cdot d_b}{4 \cdot E_s \cdot I_b}} = \sqrt[4]{\frac{153.24 \cdot 12}{4 \cdot 210000 \cdot 1017.88}} = 0.0383 \tag{A.4}$$

$$\alpha_{\max} = \sqrt[4]{\frac{k_{c,\max} \cdot d_b}{4 \cdot E_s \cdot I_b}} = \sqrt[4]{\frac{1186.11 \cdot 12}{4 \cdot 210000 \cdot 1017.88}} = 0.0402 \tag{A.5}$$

where $E_s$ is the steel elastic modulus and $I_b$ the second moment of area of the dowel.
The global deformability of the connection ($\lambda_{\tau,lig}$) is evaluated considering the contribution of the dowel embedded in the concrete, the dowel embedded in the grout and the elastomeric cushion:

$$\begin{aligned}
\lambda_{\tau,lig} &= \left[ \frac{G_{neo} \cdot A_0}{h_n} + \left( n \cdot E_s \cdot I_b \right) \cdot \left( \frac{h_n^3}{12} + \frac{1}{3.5 \cdot \alpha_{\min}^3} + \frac{1}{3.5 \cdot \alpha_{\max}^3} \right)^{-1} \right]^{-1} = \\
&= \left[ \frac{1 \cdot 45000}{5} + \left( 2 \cdot 210000 \cdot 1017.88 \right) \cdot \left( \frac{5^3}{12} + \frac{1}{3.5 \cdot 0.0383^3} + \frac{1}{3.5 \cdot 0.0402^3} \right)^{-1} \right]^{-1} = \\
&= 18.51 \cdot 10^{-6} \ mm/N
\end{aligned} \tag{A.6}$$

$G_{neo}$, $A_0$ and $h_n$ are the shear modulus, the bearing area and the thickness of the elastomeric cushion, $n$ is the number of dowels.
Point A and B in Figure A1 are related to considerations of dowels embedded in the mortar ($F_{vy,min}$) and in the concrete ($F_{vy}$), respectively. Those values are obtained from the following calculations:

$$\varepsilon_{\min} = \frac{3 \cdot e}{d_b} \cdot \sqrt{\frac{f_{ck,\min}}{f_{sy,red}}} = \frac{3 \cdot 2.5}{12} \cdot \sqrt{\frac{40}{238}} = 0.256 \tag{A.7}$$

$$\begin{aligned}
C_{e,\min} &= \sqrt{1 + \left( \varepsilon_{\min} \cdot C_{1,\min} \right)^2} - \varepsilon_{\min} \cdot C_{1,\min} = \\
&= \sqrt{1 + \left( 0.256 \cdot 1.18 \right)^2} - 0.256 \cdot 1.18 = 0.7424
\end{aligned} \tag{A.8}$$

$$\begin{aligned}
F_{vy,\min} &= C_r \cdot C_{e,\min} \cdot C_{1,\min} \cdot n \cdot d_b^2 \cdot \sqrt{f_{ck,\min} \cdot f_{sy,red}} = \\
&= 1 \cdot 0.7424 \cdot 1.18 \cdot 2 \cdot 12^2 \cdot \sqrt{40 \cdot 238} = 24616 \ N
\end{aligned} \tag{A.9}$$

$$\varepsilon_{\max} = \frac{3 \cdot e}{d_b} \cdot \sqrt{\frac{f_{ck,\max}}{f_{sy,red}}} = \frac{3 \cdot 2.5}{12} \cdot \sqrt{\frac{59}{238}} = 0.3112 \tag{A.10}$$

$$\begin{aligned}
C_{e,\max} &= \sqrt{1 + \left( \varepsilon_{\max} \cdot C_{1,\max} \right)^2} - \varepsilon_{\max} \cdot C_{1,\max} = \\
&= \sqrt{1 + \left( 0.3112 \cdot 1.25 \right)^2} - 0.3112 \cdot 1.25 = 0.6840
\end{aligned} \tag{A.11}$$

$$F_{vy} = C_r \cdot C_{e,\max} \cdot C_{1,\max} \cdot n \cdot d_b^2 \cdot \sqrt{f_{ck,\max} \cdot f_{yk}} = \\ = 1 \cdot 0.6840 \cdot 1.25 \cdot 2 \cdot 12^2 \cdot \sqrt{59 \cdot 250} = 29180\ N \tag{A.12}$$

where $e$ is the eccentricity of the shear force and $f_{yk}$ is the tensile strength of the dowels. $C_r$, $C_{1,max}$ and $C_{1,min}$ are constants (Ferreira, 1999) depending on the connection degree of fixity and on the ultimate strength of grout/concrete.

The displacement $a_{v,min}$ is obtained from the global deformability of the connection and $F_{vy,min}$:

$$a_{v,\min} = \lambda_{\tau,lig} \cdot F_{vy,\min} = 18.5 \cdot 10^{-6} \cdot 24616 = 0.46\ mm \tag{A.13}$$

The length of the plastic hinge ($l_p$) in dowels is a function of the reduced steel strength ($f_{sy,red}$):

$$x_1 = \frac{\sqrt{f_{sy,red} / f_{ck,\min}}}{3 \cdot C_{1,\min}} \cdot d_b = \frac{\sqrt{238/40}}{3 \cdot 1.18} \cdot 12 = 8.27\ mm \tag{A.14}$$

$$x_2 = \frac{\sqrt{f_{sy,red} / f_{ck,\max}}}{3 \cdot C_{1,\max}} \cdot d_b = \frac{\sqrt{238/59}}{3 \cdot 1.25} \cdot 12 = 6.43\ mm \tag{A.15}$$

$$l_p = x_1 + x_2 + h_n = 8.27 + 6.43 + 5 = 19.70\ mm \tag{A.16}$$

The displacement associated with $F_{vy}$ is obtained from:

$$\alpha_{crit} = 1750 \cdot \frac{f_{sy,red}}{d_b \cdot E_s} = 1750 \cdot \frac{238}{12 \cdot 210000} = 0.165 \tag{A.17}$$

$$a_{vy} = \alpha_{crit} \cdot l_p = 0.165 \cdot 19.70 = 3.26\ mm \tag{A.18}$$

The ultimate strength of the dowels is:

$$F_{v,tot} = C_1 \cdot n \cdot d_b^2 \cdot \sqrt{f_{ck,\max} \cdot f_{sy,red}} = 1.03 \cdot 2 \cdot 12^2 \cdot \sqrt{59 \cdot 238} = 35152\ N \tag{A.19}$$

The displacement associated with $F_{v,tot}$ is obtained from interpolation:

$$\frac{29179 - 24616}{3.26 - 0.46} = \frac{35152 - 24616}{a_{v,tot} - 0.46} \Rightarrow a_{v,tot} = 6.92\ mm \tag{A.20}$$

Finally, the maximum displacement is assumed equal to the dowel diameter:

$$a_{v,\lim it} = d_b = 12\ mm \tag{A.21}$$

**Figure A2** shows the resulting shear-displacement diagram.

The moment-rotation relationship is calculated for clockwise and counter-clockwise bending moments, as described in section 4. The first step consists in the evaluation of the yield moment ($M_y$ = 6.25kNm) associated with yielding of the dowels obtained from a cross-section analysis. The corresponding values of the neutral axis ($x$) and the axial strain in the dowels ($\varepsilon_s$) are 3.84cm and 0.125%, respectively.

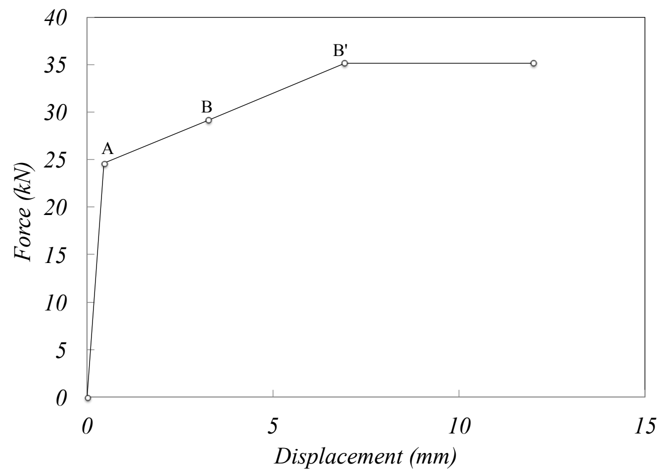


***Figure A2*** *– Force-displacement relationship for the connections of case study A*

The axial deformation of the dowels associated with the applied post-tension is $\varepsilon_{s,post} = 0.0875\%$. The corresponding rotation ($\varphi_y$) is obtained from considering a constant deformation along the dowel length ($l_s$):

$$\begin{aligned}\varphi_y &= \varphi_y - \varphi_{y,post} = \frac{\varepsilon_s \cdot l_s}{d_s - x} - \frac{\varepsilon_{s,post} \cdot l_s}{d_s - x} = \\ &= \frac{0.00125 \cdot 750}{150 - 38.37} - \frac{0.000875 \cdot 750}{150 - 38.37} = 2.52 \cdot 10^{-3} \ rad\end{aligned} \tag{A.22}$$

Similarly, the second step consists in the calculation of the ultimate moment ($M_u$ = 11.08kNm), the corresponding neutral axis ($x_u$ = 10.9cm) and the dowel strain ($\varepsilon_{su}$ = 2.049%).

The corresponding rotation ($\varphi_u$) is:

$$\begin{aligned}\varphi_u &= \varphi_u - \varphi_{y,post} = \frac{\varepsilon_{su} \cdot l_s}{d_s - x_u} - \frac{\varepsilon_{s,post} \cdot l_s}{d_s - x} = \\ &= \frac{0.02049 \cdot 750}{150 - 10.94} - \frac{0.000875 \cdot 750}{150 - 38.37} = 104.63 \cdot 10^{-3} \ rad\end{aligned} \tag{A.23}$$

For counter-clockwise rotations, the contact between the top of the beam and the side of the column can be reached. The available rotation $\varphi_{av}$ before contact is:

$$\varphi_{av} = \frac{gap}{H + h_n} = \frac{20mm}{500mm + 5mm} = 39.60 \cdot 10^{-3} \ rad \tag{A.24}$$

In this specific case the contact occurs after yielding and before reaching the ultimate moment, therefore the bending moment corresponding to beam-column contact is obtained from interpolation:

$$\frac{M_{contact} - M_y}{\varphi_{av} + \varphi_y} = \frac{M_u - M_y}{\varphi_u + \varphi_y} \Rightarrow M_{contact} = 7.98 \ kNm \tag{A.25}$$

After contact, the stiffness increases. The bending moment associated with dowel shear failure ($F_{v,tot}$):

$$M_{post-contact} = F_{v,tot} \cdot 0.9 \cdot (h+e) = 35151 \cdot 0.9 \cdot (500+2.5) = 15.90 \ kNm \quad \text{(A.26)}$$

Finally, **Figure A3** shows the resulting moment-rotation curve considered in the analyses.

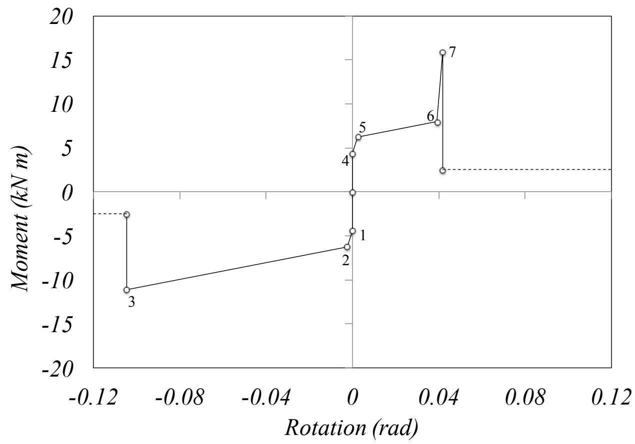


***Figure A3*** *– Moment-rotation curve for beam-column connections of Case Study A*
*Note: 1) loss of post-tension; 2) dowel yielding in tension; 3) dowel failure in tension;*
*4) loss of post-tension; 5) dowel yielding in tension; 6) beam-column contact; 7) dowel failure in shear.*